# Planar near-field measurement on an omni-directional UWB antenna

**Xuebin Hou[*(1)], Clive Parini [(1)], Stuart Gregson[(2)],**

*(1) Depart of Electronic Engineering, Queen Mary, University of London, U.K.*
*Email:xuebin.hou@elec.qmul.ac.uk c.g.parini@elec.qmul.ac.uk*

*(2) Nearfield Systems Inc. U.S.*
*Email:sgregson@nearfield.com*

**ABSTRACT:** In this paper a novel planar near-field measurement technique is used to characterise an omni-directional ultra-wideband (UWB) antenna. It is shown through numerical simulation and experimental verification that a full sphere far-field pattern of an omni-directional antenna can be obtained with planar near-field acquisition system. It offers a cost effective near-field solution to a class of antenna that currently can only be effectively served with spherical NF scanning.

## INTRODUCTION

The development of wireless communication requires accurate and cost effective measurement methods to determine the radiation pattern of the antennas in the communication system. The near-field measurement is appreciated thanks to the development of near-field scanning technique and near-field to far-field transforming algorithm.

When the electromagnetic field is known over an arbitrary surface surrounding a radiated antenna, it is possible to determine that field everywhere outside that surface including the far-field distance from the radiator. Through rigorous mathematic computation, the far-field radiation pattern of the Antenna Under Test (AUT) can be predicted including parameters such as gain, directivity, beam-width, etc from near-field probing on a surface surrounding the AUT. In near-field measurement, the probe antenna is moved by the near-field scanning robot over a path that captures microwave emissions from the AUT, the path of motion is usually constrained to a surface and in three basic geometrical surfaces surrounding the AUT can be adopted: planar, cylindrical and spherical. [1] Choosing a measurement configuration one should consider such parameters as: the AUT's shape (height, width, length etc.), its practice usage (high-directional or omni-directional) and the limitation of existing near-field measurement facility.

Compared with other measurement geometries, a planar scan surface has some advantages such as cost effective facility, simple alignment, simple probe correction and stationary AUT during scan, but is usually restricted to a rectangular scanning surface orthogonal to the z-axis of the scanner, the finite size of scanning surface introduces errors in the predicted far-field, often called the truncation error [2]. Generally, the planar scanning surface is preferred for high gain antennas because all significant plane-wave energy is typically within $10°$ of the boresight axis and spherical or cylindrical scanning surface is always considered to serve low gain antennas because the energy should be captured at large angles from the AUT boresight axis [3].

To overcome the limitation of truncation error of planar near-field geometry, a novel method "poly-planar near-field measurement" [4], has been developed at Queen Mary, University of London (QMUL). This technique attempts to reduce or even remove truncation errors by construction of a polyhedral sampling surface that encloses the AUT, from a set of partial scans that taken individually fail to fulfil the transformation requirements in terms of continuity over the sampling interval. The poly-planar technique brings improvements to planar near-field measurement method: it extends the planar technique so that it can applied to low gain antennas as well as high gain antennas and the directivity, total radiated power and radiation efficiency of an AUT can be accurately characterized using essentially a conventional planar facility with a modified AUT positioner and transform software. Thus success of the poly-planar technique means the potential ability for small planar scanner facilities to be fully explored and the costs of updating near-field scanning facilities can be reduced.

With the success of poly-planar technique on directional antenna, it is considered that a full sphere far-field pattern of an omni-directional antenna may be predicted with planar near-field acquisition system, and this is the object of this paper.

## CUBE PLANAR NEAR-FIELD MEASUREMENT ON AN UWB ANTENNA

From Kirchhoff-Huygens formula:

$$e(u) = \frac{\pi}{j\lambda^2}\int_s [u\times(n\times E_0) + Zu\times[(n\times H_0)\times u]]\exp(jku\cdot r_0)da \qquad (1)$$

It is clear that the far-field vector pattern function $e(u)$ can be derived with integral of the field $E_0$, $H_0$ over a closed surface S [5]. This means if both the electric and magnetic field around AUT had been specified, the whole sphere far-field pattern of AUT can be determined. In this paper, the chosen AUT is a cpw-fed circular discmonopole UWB antenna, see Fig.1, which is designed and fabricated at QMUL [6]. Its merits such as omni-directional pattern, compact and small dimension ($47mm\times 40mm\times 1.6mm$) are suitable for investigating this novel method.

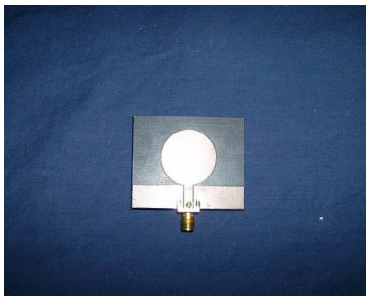

**Fig. 1 Photograph of a monopole disk UWB antenna.**

The investigation begins with simulation in CST Microwave studio. Six monitor planes has been located at x=72mm, x=-72mm, y=72mm, y=-72mm, z=72mm and z=-72mm, they compose an imaginary cube 144mm×144mm×144mm and enclose the AUT with the center point located at (0,0,0). Fig. 2(a) illustrates the cube, Fig. 2(b) and Fig. 2(c) illustrate amplitude and phase of electric field $E_y$ distribution on it at 9GHz.

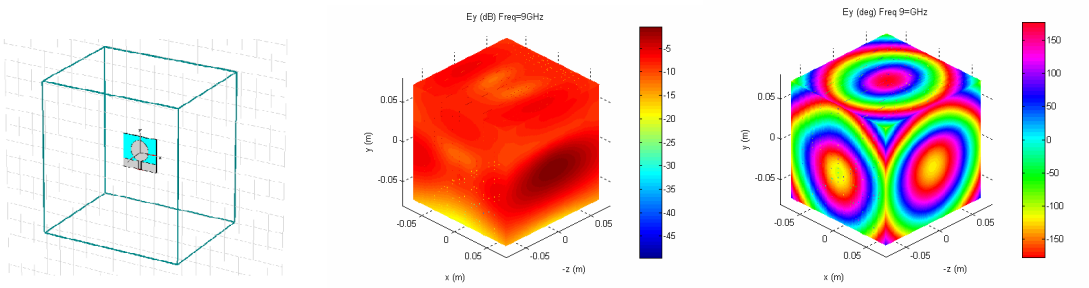


**Fig. 2(a) (b) (c) E-field distribution on cube scanning box at 9GHz**

When both electric and magnetic field on the cube have been calculated, the corresponding far-field pattern can be constructed. The constructed far-field pattern and simulated far-field pattern is shown in Fig.5 below together with experimental result.

**EXPERIMENTAL VERIFICATION AND IMPROVEMENT**

A series of measurement have been taken in QMUL Antenna Laboratory to implement the poly-planar technique on this circular discmonopole UWB antenna. To acquire all six planes of the imaginary cube, the AUT is fixed on a special six position mount that enable the required $90°$ rotation about x-axis and y-axis to be made while keeping alignment with the axis of the range as shown in Fig.3.

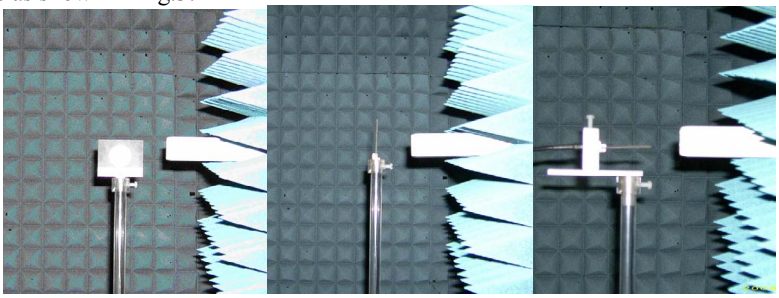

**Fig. 3 Planar near-field scanning on AUT**

The probe involved in this measurement is NSI WR90, a standard medium gain waveguide probe, suitable for frequency 8.2GHz-12.4GHz x-band frequency range. The measurements here were taken at 9GHz. The acquired planar near-field data set contains amplitude and phase distribution for two orthogonal polarization components, which are all tangential with the measurement plane. It is not the real tangential component radiated by AUT, because the true angular response of AUT is distorted by the convolution between the AUT and probe angular responses. Thus, probe pattern correction should be implemented to acquire the real tangential components $E_x$ and $E_y$. To specify the electric

field on the measurement plane, the normal field components $E_z$ has to be obtained by applying the plane-wave condition to the angular spectra [4]:

$$E_z = -f^{-1}\{\frac{k_x f(E_x) + k_y f(E_y)}{k_z}\} \quad (2)$$

Here $f$ is used to denote the Fourier operator and $f^{-1}$ its inverse, the Fourier transform is used to convert a phase front acquired through near-field measurement into equivalent angular energy distribution at the location and vice versa for the inverse Fourier transform. The reconstructed normal field component $E_z$ on the cube box is plotted in Fig.4, although there are still some discontinues at intersection between adjacent planes, most of them match well.

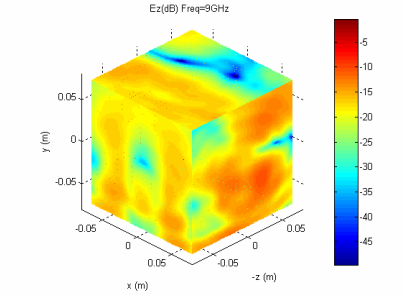


**Fig. 4 Constructed normal field component**

After the magnetic field has been calculated through electric field, the far-field pattern can be predicted, as shown in Fig.5 (a), together with simulation results Fig 5(b), here Fig 5(b) is far-field pattern derived from simulated near-field results.


**Fig. 5(a) (b) Constructed far-field pattern through near-field scanning and near-field simulation**

Noting the similarity between far-field prediction based on experimental and simulated near-field results (Fig. 5(a) and Fig. 5(b)), this near-field scanning method may have a great deal of refinement. The inaccuracy in far-field pattern arise form high field intensity among boundary of adjacent planes. If replaced the square cube box with a flat cube box in near-field scan, then most energy will concentrate on two planes, there will be relatively lower field intensity among boundary, and the angular spectrum arising from integral of near-field will most attribute to the 2 major planes. Fig.6 shows $E_y$ amplitude distribution on 2 kinds of flat cube box with AUT been set in middle of its inside, their sizes described in $x \times y \times z$ are: $240mm \times 240mm \times 40mm$ for Fig.6(a) and $60mm \times 240mm \times 240mm$ for Fig.6(b).

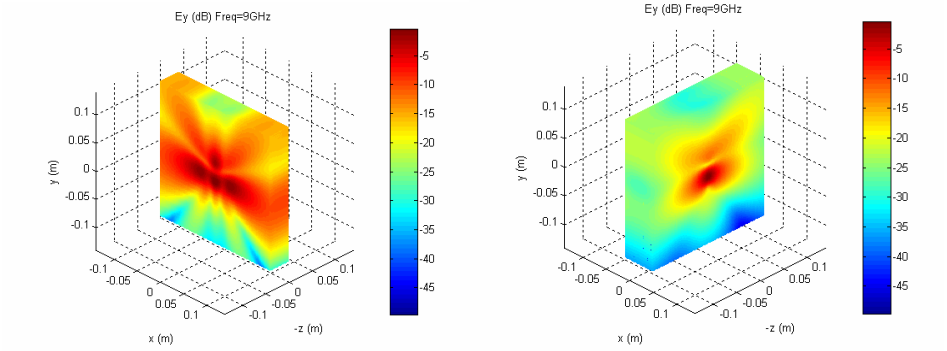


**Fig. 6(a) (b) Simulated E-field distribution on flat cube box**

And far-field patterns derived from near-field distribution on flat cube boxes above are shown in Fig.7 (a) and Fig. 7(b), together with direct far-field simulation shown in Fig. 7(c). The improvement in reliability is obvious.

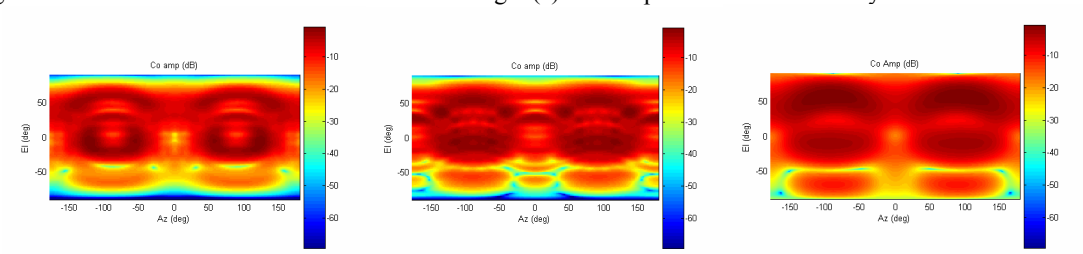


**Fig. 7(a) (b) (c) Constructed far-field pattern through near-field simulation (a,b)and far-field simulation(c)**

Fig.8 shows the far-field pattern at great-circle cut on Elevation= $0°$ comparison between simulation and measurement taken in both near-field and far-field. Here, the blue trace (data 1) represents far-field prediction based on near-field simulation result shown in Fig.6 (b); the green trace (data 2) represents far-field simulation; the red trace (data 3) represents far-field prediction derived from near-field scanning; and the black trace (data 4) corresponds to direct far-field measurement result.

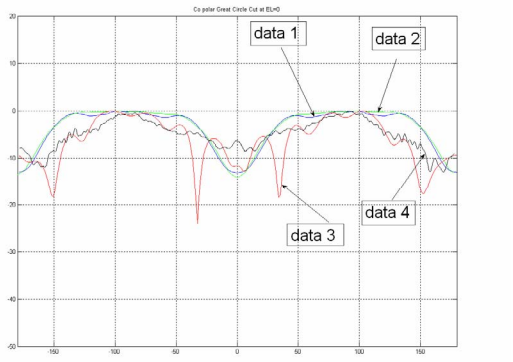


**Fig. 8 Far-field great-circle cut comparison between different processes**

## CONCLUSION

Through numerical simulation and experimental verification, encouraging preliminary results has been obtained. The work offers a possibility to manage a planar near-field measurement on an omni-directional antenna, which currently can only be effectively served with spherical near-field measurement system.

**ACKNOLEGEMENT:** The authors would like to thank Mr. John Dupuy of the Department of Electronic Engineering, QMUL for his help in the fabrication and measurement of the antenna, and also would like to acknowledge Computer Simulation Technology (CST), Germany, for the complimentary license of the CST Microwave Studio package.

## REFERENCES

[1] Yaghjian,A.: 'An overview of near-field antenna measurement'. IEEE Transactions on Antennas and Propagation, Volume 34, pp.30 – 45, Jan.1986

[2] A. C. Newell.: 'Error analysis techniques for planar near-field measurements," IEEE Trans. Antennas and Propagation, Volume 36, pp.754–768, Jun.1988.

[3] Dan Slater.: 'Near-Field Antenna Measurement'. 1991 Arctech House, Inc. pp32

[4] Gregson, S.F.; Parini, C.G.; McCormick, J.: 'Development of wide-angle antenna pattern measurements using a probe-corrected polyplanar near-field measurement technique', Microwaves, Antennas and Propagation, IEE Proceedings, pp.562-571, Dec.2005

[5] R.H.Clarke and John Brown. 'Diffraction theory and antennas'. 1980 Ellis Horwood, Inc. pp227

[6] Jianxin Liang; Chiau, C.C; Xiaodong Chen and Parini, C.G.: 'Study of a printed circular disc monopole antenna for UWB systems'. IEEE Transactions on Antennas and Propagation, Volume 53, Issue 11, pp.3500 – 3504, Nov.2005